Fast infrared imaging spectroscopy technique (FIIST)

ARTICLE *in* INFRARED PHYSICS & TECHNOLOGY · JANUARY 2015

Impact Factor: 1.55 · DOI: 10.1016/j.infrared.2014.12.005

Infrared Physics & Technology 68 (2015) 152–158

Contents lists available at ScienceDirect

Infrared Physics & Technology

journal homepage: www.elsevier.com/locate/infrared

Fast infrared imaging spectroscopy technique (FIIST)

M. Romano [a,*], C. Ndiaye [a], A. Duphil [a], A. Sommier [a], J. Morikawa [c], J. Mascetti [b], J.C. Batsale [a], L. Servant [b], C. Pradere [a,*]

[a] I2M, Département TREFLE, UMR CNRS 5295 – site ENSAM, Esplanade des Arts et Métiers, 33405 Talence Cedex, France
[b] ISM, Institut des Sciences Moléculaires, UMR CNRS 5255, Université de Bordeaux, 351 cours de la Libération, 33405 Talence cedex, France
[c] Tokyo Institute of Technology, Department of Organic and Polymeric Materials, Tokyo, Japan

HIGHLIGHTS

- Development of a novel infrared imaging spectroscopy technique.
- Focal plane array spectral characterization.
- Comparison of spectra with a reference spectrometer.
- Fast infrared imaging spectroscopy technique (FIIST).

ARTICLE INFO

Article history:
Received 12 November 2014
Available online 9 December 2014

Keywords:
Infrared thermography
Imaging
Spectroscopy
Focal plane array (FPA)

ABSTRACT

We describe an infrared multispectral imaging spectrometer capable of monitoring up to 76,800 spectra in less than 3 min. In this article, measurements collected using this set-up are presented and discussed, emphasizing the resolution (spatial and temporal), accuracy and capabilities of the instrument. Finally, some applications of multispectral imaging are presented.

1. Introduction

An infrared multispectral imaging spectrometer is an instrument that can simultaneously record spectral, spatial and temporal information of a sample by measuring the intensity variation of a signal due to molecular vibrations. Objects are composed of vibrating atoms, and some of these atoms have higher energy and vibrate more frequently. The vibration of all charged particles and atoms generates electromagnetic waves. When the temperature of an object increases, the vibration of the atoms becomes faster, and thus, the spectral radiant energy rises. As a result, all radiation emitted by the object is a function of the wavelength distribution according to the temperature. This type of information is of particular interest because chemical and thermal properties of materials are strongly coupled in many applications. Chemical characterization is typically achieved by using analytical spectroscopy methods. Most of these techniques have proved to be well suited for quantitative measurements; moreover, the techniques allow for characterization by scanning the surface of a sample. This scanning technique is difficult to use due to problems associated with transient characteristics. As a result, considerable efforts have been made in the past few years to develop multispectral imaging instruments [1–6]. Also some recent work which takes into account the time-resolved coupled conducto-radiative heat transfer and the temperature of experiments [7]. The main objective remains to be able to read the chemical content at each pixel of an image by visualizing the sample composition. In this respect, infrared (IR) spectroscopy has characteristic advantages, such as high speed (one minute or less per sample); non-destructive, non-intrusive character; high penetration of the probing radiation beam; suitability for on-line use; and nearly universal application. The combination of these characteristics with instrumental control and data treatment allow for the expansion of the domain of IR technology [8–10]. Many studies concerning the evaluation of near-infrared (NIR) spectroscopic imaging as a tool have been published with respect to pharmaceutical applications [11], food [12], polymers [13] characterization and even to quantify hydrated silica on Mars [14]. In addition, other breakthroughs have been reported by using high-resolution infrared imaging systems for medical applications [15]. In this type of system, the thickness of

* Corresponding authors.
E-mail addresses: romano@enscbp.fr (M. Romano), c.pradere@i2m.u-bordeaux1.fr (C. Pradere).

http://dx.doi.org/10.1016/j.infrared.2014.12.005
1350-4495/

the sample layer has to be adjusted to improve the penetration depth of IR radiation. For miniaturized applications, it is important to increase local spatial resolution; in this case, field stops are used to limit the "field of vision" of the infrared beam to the interesting areas of a sample. In contrast, for the analysis of large samples (larger surfaces) with high spatial resolution, it is necessary to move the sample step by step by using a motorized sample support. Then, spectra of the different areas are recorded one after the other. This conventional procedure, often termed mapping, is extremely time-consuming such that mapping a sample area of 2.1×2.1 μm at a spatial resolution of 6.21 μm takes approximately 21 h [15]. In contrast, Chan and Kazarian characterize chemical reactions by using a faster methodology [16].

In this study, an IR broadband Bentham monochromator (operating with a wavelength ranging from 1 to 21 μm) and a MWIR (mid-wavelength infrared) InSb (indium antimonide) infrared camera (from 2 to 6 μm) were combined to develop a fast infrared imaging spectroscopy technique (FIIST). To analyze the performance of this new instrument, it was necessary to choose a standard reference to enable the comparison and to validate the technique. To this end, a Bruker Vertex 70v spectrometer was used as the reference instrument to describe the performance of FIIST in terms of spectral chemical characterization. In this work, the FIIST instrumentation is presented and its performance is compared to that of the Bruker instrument. In this particular application, FIIST was submitted to a validation process to confirm that the chemical spectra were in good agreement with the reference spectra. After describing the experimental set-up, this paper will presents the results obtained for model samples using the new instrument. This section involves the characterization of the infrared detector over its wavelength range, followed by a comparison of the spectra obtained for different materials by the two techniques to demonstrate that the spectra obtained with the new instrument are consistent with the reference spectra. Finally, it is discussed how, based on the combination of these technological advances, FIIST is a versatile and flexible technique due to its homemade characteristic.

2. Materials and methods

2.1. Experimental set-up

The multispectral imaging instrument developed in this study is schematized in Fig. 1. The instrument is composed of a Bentham monochromator (Tmc300) for sample analysis. Furthermore, the instrument is equipped with a multispectral lamp (Nernst and halogen) emitting from 400 nm to 20 μm and with three gratings allowing for the wavelength to be tuned, which are mounted on a rotated turret for mechanical adjustment. Order sorting filters are used to ensure that only the first diffraction order is transmitted. In this application, two blazed gratings with 150 and 300 grooves are used to scan over a broad infrared band ranging from 2 to 6 μm in 1 nm steps. The optical path of the beam inside the spectrometer is controlled by two parabolic mirrors and two planar mirrors. The beam emitted from the slit (Fig. 1) is monochromatic. In fact, this source light is transmitted through the sample and recorded by the IR camera used as a sensor. The IR camera is an FLIR SC7000, InSb focal plane array (FPA) composed of 76,800 individual sensors (FPA composed of 240×320 pixels and pitch size of 25 μm × 25 μm) with a 25 mm objective and a MWIR F/2 focal length the spatial resolution is about 200 μm. Nevertheless, if other IR objectives are used spatial resolution can be upgraded. Thus, in transmission mode, the camera is placed behind the sample as shown in Fig. 1 (element 13). The acquisition frequency reaches up to 1 kHz. The acquisition of infrared spectra is achieved by the synchronization of the monochromator and the IR camera by homemade Labview and Matlab software to control the acquisition frequency and to scan the wavelength over the domain of interest. The same software also facilitates frame recording and data saving in appropriate formats for post-processing. A calibration protocol is given by Bentham for the alignment of the optical set-up and also for the lamps. For insuring the transmission of the wavelengths reference standards materials we used to calibrate the proposed instrument.

2.2. Characteristics of the reference instrument

A Bruker Vertex 70v equipped with a globar light source (stick of SiC) is used as a reference instrument. This apparatus is equipped with a beam splitter broadband MIR-FIR (Mid InfraRed – Far InfraRed) made of silicon (6000–10 cm^{-1} range or 1.66–1000 μm) and a DLaTGS/CsI (deuterated L-alanine-doped triglycine sulfate/cesium iodide) detector, which can operate over a wide range of frequencies, i.e., 6000–130 cm^{-1} (1.66–76 μm). The equipment allows for acquisition at high speeds of up to 56 spectra per second due to the rapid scan modules. The standard spectral resolution is of the order of 0.4 cm^{-1}. However, depending on the application, the spectrometers sensitivity can be upgraded (in terms of energy) by decreasing the spectral resolution to 16 cm^{-1}. This spectrometer is used in transmission mode.

2.3. Performances in the spectral domain of interest

The spectral domain of interest is determined by the infrared camera detector. Thus, the comparison of the two instruments will

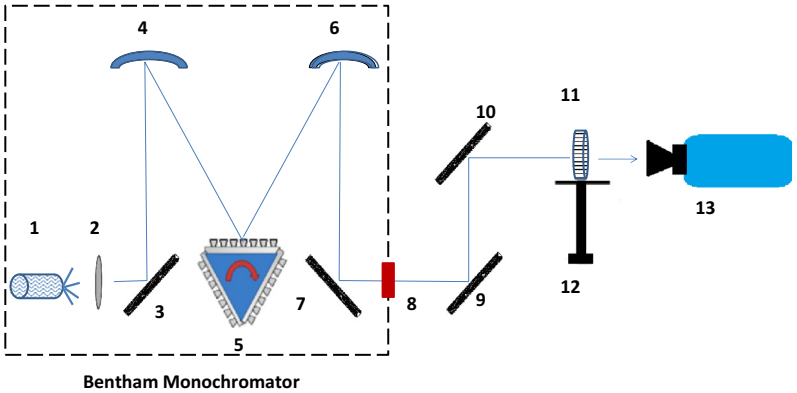

Fig. 1. Scheme of the experimental set-up in vertical transmission mode, composed of Bentham spectrometer (elements from 1 to 7): (1) Multispectral Nernst lamp. (2) Order sorting filters wheel (3) Planar mirror. (4) Parabolic mirror. (5) Tunable grating. (6) Parabolic mirror. (7) Planar mirror. (8) Slit. (9,10) Parabolic mirrors. (11) Sample. (12) Sample holder. (13) Infrared InSb cooled camera.

Table 1
Configuration of both spectrometers.

	Light source	Detector	Speed acquisition (spectra/s)	Spectral resolution v (cm^{-1})	Wavelength resolution λ (μm)
Bruker vertex 70v	Globar	DLaTGS/CsI	56	0.4	–
This instrument	Nernst	InSb	320	–	0.001

Table 2
Vibrational spectroscopy detector specifications. Note that the detector element of DLaTGS/CsI is a cylinder; thus, the given size corresponds to the diameter.

Detector element/window	Element size	Spectral range v (cm^{-1})	Wavelength range λ (μm)	Typical D^* ($cmHz^{1/2}\,W^{-1}$)	Operating temperature (K)
DLaTGS/CsI	1.3 mm	6000–130	1.66–76	$2.4e^8$	Room temp.
InSb	25 μm	5000–1850	2–5.4	$2.2e^{11}$	77, Stirling

be limited to this field. The characteristics of the two devices are summarized in Table 1.

It is important to note that the spectral range of the developed instrument is determined by the following optical properties of the Bentham monochromator: linear dispersion 2.7 nm/mm and wavelength accuracy ±0.2 nm. The acquisition rate is limited by the mechanical displacement of the monochromator.

The specific detectivity, (D^*), for a photo quantum detector is used to characterize its performance. This parameter corresponds to the measure of the detector signal as a function of energy flux and detector noise and is equal to the reciprocal of the noise-equivalent power (NEP); furthermore, the specific detectivity can be defined as the minimum power that a detector senses for a filter bandwidth ($\Delta\lambda$) with a 1 cm^2 area and 1 Hz acquisition rate [17,10]. In this study, the InSb detector exhibited a D^* value of $2.2e^{11}$ $cmHz^{1/2}\,W^{-1}$ (data from FLIR), making it more than 900 times more sensitive than the DLaTGS detector, which shows a D^* value of $2.4e^8$ $cmHz^{1/2}\,W^{-1}$ (data from BRUKER). For this reason, the spatial resolution is determined by the size of the detector element. The reference instrument was used to acquire spectra from an infrared spot size (incident beam spot, on the order of millimeters) on a sample. The specifications of the vibrational spectroscopy detectors are summarized in Table 2. It is important to note that the reference instrument was not built for imaging purposes; therefore, in this particular comparison, the observed ratio between the D^* values, i.e. 900, can be related to the technological differences of the element detectors. The purpose of this comparison is to better describe the performance of FIIST by referring to the Bruker device as the standard instrument. In addition, the InSb detector is composed of a focal plane array (FPA) featuring 76,800 (320 × 240) pixels acting as independent sensors, and the simultaneous measurement of 76,800 spots can be performed under snapshot mode in 1 μs.

2.4. Materials

For this study, thin plastic films were chosen as samples to analyze homogeneous fields of chemical species. The measurements were performed in transmission mode, and the analyzed samples' thickness ranged from 3 to 110 μm. In the experiments, the spectral characterization of polystyrene (PS, 110 μm thickness), polyethylene (PE, 3 μm thickness) and a printed transparency film was performed.

2.5. Spectrum acquisition

The transmission mode spectrum analysis is schematized on Fig. 1, and a more detailed scheme is shown in Fig. 2. The FPA was used to generate an imaging area of 2 cm × 1 cm; a visible image of the plastic film holder is shown in Fig. 2A. The framed area shows the position of the thin plastic film. An infrared image of the same sample holder at a wavelength of 3 μm is shown in Fig. 2B. This is a typical infrared image obtained by spectral analysis. It is important to note that for each wavelength, one image or a sequence of images can be obtained to improve the signal-to-noise ratio. Because each pixel represents a detector, a scheme of the infrared image (Fig. 2B) with the superposition of the acquisition pixel matrix over the frame area is shown in Fig. 2C. It should be noted that a matrix of 320 × 240 pixels covers a sample surface area of 3 × 1.5 cm for a spatial resolution of ≈200 μm. Considering the characteristics of the sample surface, a pixel line was selected from the spectral cartography, as shown in Fig. 2D. In this three-dimensional plot, the absorbance response for each pixel of the previously selected line is shown as function of wavelength from 2 to 6 μm. Because the material is a homogenous thin film, the same spectrum was observed at each pixel. Every pixel of this image contains the spectral response function of the wavelength of the material (Fig. 2B). In addition, even if the spectrum acquisition is limited by the mechanical displacement of the monochromator, the overall acquisition of the spectra remains fast (less than 3 min), with approximately 76,800 spectra acquired between 2 to 6 μm with a 1 nm step size, which corresponds to 300 million data points.

3. Experimental results and discussion

3.1. Characterization of the infrared sensor

This section addresses the characterization of the infrared sensor. The calibration of the detector involves the recognition of the reference background over the entire spectral range. Therefore, the incident multispectral wavelength of the spectrometer was first performed, as shown in Fig. 3 (solid line). It is important to note that the cameras intensity level was strongly dependent on both the integration time and the acquisition frequency. For this reason, the measured spectrum was normalized by the maximum value over the entire measurement range, and the initial baseline was subtracted due to the surrounding temperature. This reference spectrum (I_0) was compared to the reference spectrum acquired by the reference instrument (dashed line); it is important to note that this comparison was limited to the cameras spectral domain (spectral range of Bruker ranges from 1 to 76 μm). Fig. 3 shows that the sensitivity of the InSb detector is much better in the spectral domain of interest.

To study the effect of the noise on the spectrum acquisition, the signal-to-noise ratio (SNR) was estimated as the ratio of the mean pixel value (at each wavelength over 1000 images) to the standard deviation of the pixel values, $SNR = \mu/\sigma$, where μ is the signal mean and σ is the standard deviation noise. The SNR value was determine to be on the order of 1000, as illustrated in Fig. 4.

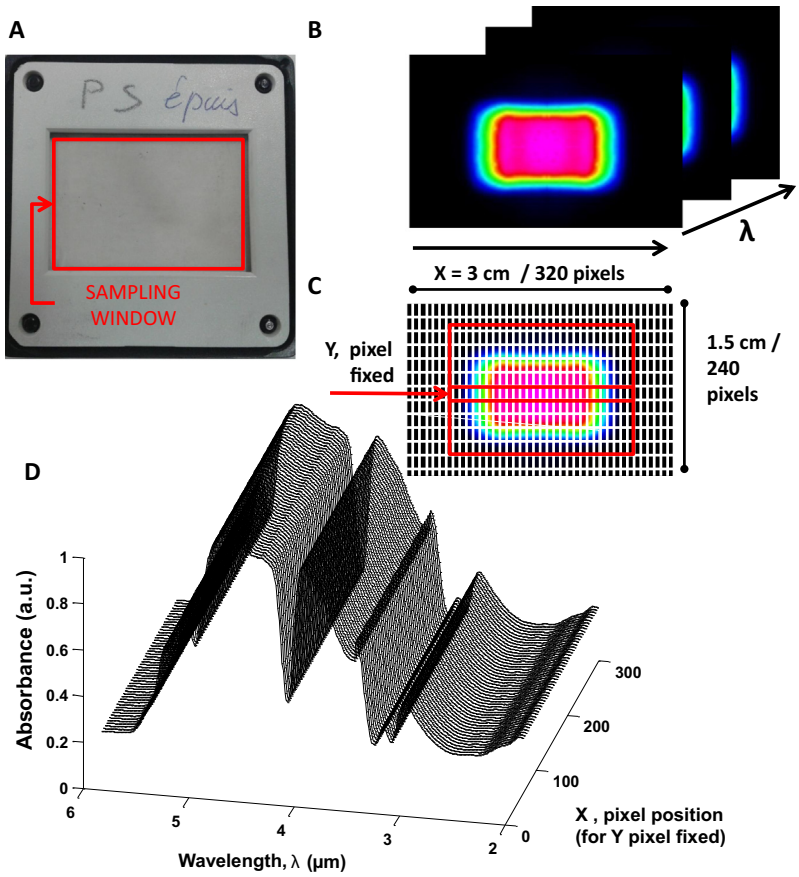

Fig. 2. (A) Thin plastic film holder (a frame is outlined to reveal the film position). (B) Infrared image of the plastic holder at a wavelength of 3 μm; note that an IR image is acquired as function of the wavelength. (C) Scheme of the infrared image with the superposition of the acquisition pixel matrix over the frame area; here, a pixel on the *Y* axis is fixed (depicted by the line) for the spectral cartography. (D) Three-dimensional plot of the material absorbance response as a function of wavelength from 2 to 6 μm; the spectrum at each pixel over the line is indicated by the *Y* fixed pixel and the *X* pixel position from 50 to 250.

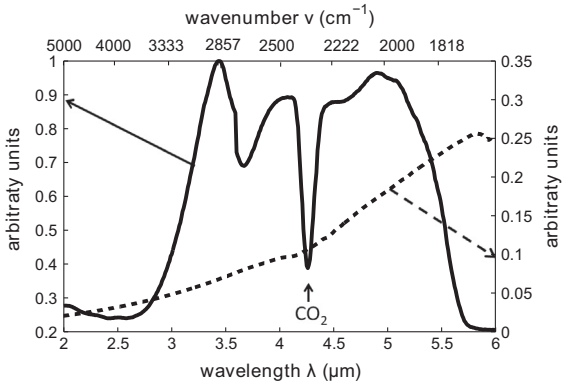

Fig. 3. Average absorbance of the FLIR SC 7000 MWIR InSb camera detector (solid line) and the Bruker Vertex 70v (dotted line) as a function of wavelength. Note that the background spectrum of the Bruker spectrometer is limited to the spectral domain of the IR camera. In addition, atmospheric CO_2 absorption can be observed at 4.3 μm (2325.6 cm^{-1}) [18] because the camera was operated under ambient conditions, whereas the Bruker features a compensation chamber (full of nitrogen) to prevent absorption due to CO_2.

3.2. Validation of the experimental set

In this section, the results of the validation process are reported. Spectra were acquired by both instruments and then compared. Specifically, the FIIST spectra were acquired using an integration time of 100 μm and a frequency of 25 Hz. Eq. (1) describes the transmittance *T*, where I_0 is the intensity of the incident radiation (background) and *I* is the intensity of the radiation emanating from the sample. The transmission spectra of the materials will be compared based on the transmittance of the samples, which is reported as a percentage.

$$T(\%) = \frac{I}{I_0} * 100(\%) \quad (1)$$

A polyethylene thin film (PE, 3 μm thickness) was selected for analysis because it is the simplest polymer structure; the polymer is a chain of methylene units terminated at each end by methyl groups. Because the polymer is completely composed of methylene groups, its chemical formula is $(C_2H_4)_nH_4$. Thus, the IR spectrum is expected to contain mainly peaks attributed to the stretching and bending vibrations of methylene. The spectra obtained by the two spectrometers are shown in Fig. 5. The spectra show good agreement. Indeed, the PE infrared bands can be observed in both spectra, where two sharp peaks dominate the spectra in the spectral region of interest: methylene stretching bands at 2920 (3.42 μm) and 2850 cm^{-1} (3.5 μm). Furthermore, it is important to note that the spectrum obtained by FIIST (Fig. 5, solid line) shows higher sensitivity for the detection of methylene stretching bands under the operating conditions.

When the side group on the methylene chain is an aromatic ring (polystyrene, PS $(C_8H_8)_n$), the infrared spectrum becomes a combination of peaks attributed to methylene and mono-substituted aromatic rings. The spectra of a PS film (110 μm thickness) obtained by the two spectrometers are shown in Fig. 6 and are in good agreement. The polystyrene infrared bands can be observed

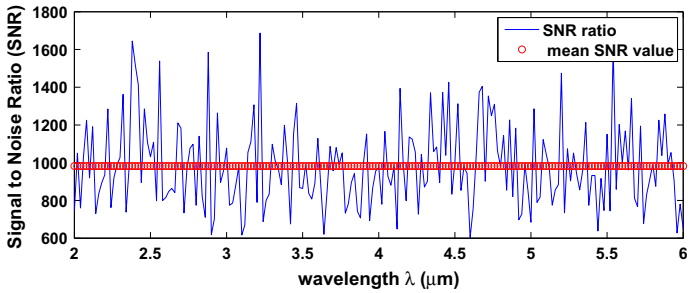

Fig. 4. Signal-to-noise ratio for each wavelength is represented by the dashed line; the average value is represented by circles, measured at 100 μm integration time.

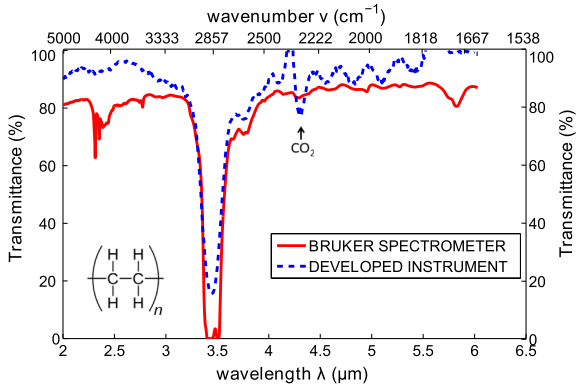

Fig. 5. Transmittance spectra of polyethylene (PE, 3 μm thickness) obtained by the Bruker spectrometer (solid line) and by the developed instrument (dashed line). Note that atmospheric CO_2 absorption can be observed at 4.3 μm (2325.6 cm^{-1}). The chemical structure of PE is schematized in the bottom left of the figure.

in both spectra, such as bands associated with =C—H stretching in aromatic rings at 3100–3000 cm^{-1} (3.22–3.33 μm). It is important to note that this frequency is slightly higher than that associated with —C—H stretching in alkane hydrocarbon chains, which occurs below 3000 cm^{-1} (3.33 μm). Aromatic hydrocarbons show other absorptions bands in the regions 1600–1585 cm^{-1} (6.25–6.3 μm) and 1500–1400 cm^{-1} (6.6–7.14 μm) due to carbon–carbon stretching vibrations in aromatic rings but are beyond the spectral range of the IR camera. In addition to bands associated with C—H stretching above 3000 cm^{-1}, two other regions associated with aromatic rings can be distinguished from the region attributed to aliphatic compounds from 2000 to 1665 cm^{-1} (5–6 μm) (weak bands known as "overtones"). It should be noted that some peaks between 2 and 3 μm were not detected by FIIST because they lie within the region where the camera has low sensitivity.

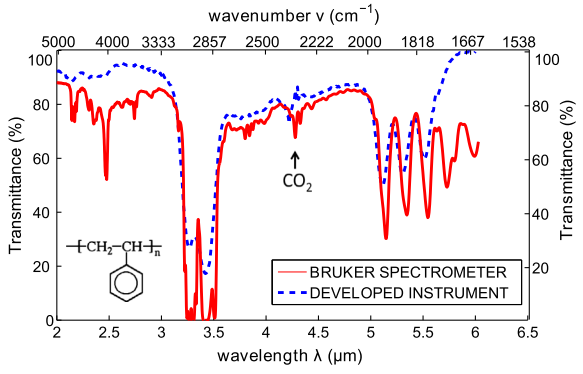

Fig. 6. Transmittance spectra of polystyrene thin film (PS, 110 μm thickness) obtained by the Bruker spectrometer (solid line) and by the developed instrument (dashed line). Note that atmospheric CO_2 absorption can be observed at 4.3 μm (2325.6 cm^{-1}). The chemical structure of PS is schematized at the bottom left of the figure.

For both samples (PE and PS), the analytical results show that the developed instrument can analyze materials that are usually opaque to spectrometers operated in transmission mode. This feature is due the specific detectivity, D^* (900 times more sensitive), which enables the instrument to detect transmitted energy through thick samples. In addition, the differences observed between the two spectra (Fig. 6) are insignificant with respect to wavenumber accuracy because the observed shift is lower than the typical tolerance of ±1 cm^{-1}. However, the spectra can be compared with an equivalent sensitivity (in terms of wavenumber). In contrast, the resolution (in terms of energy) is observed to vary between the spectra because the instruments have different sensitivities to both the thickness and the scattering properties of the thin films. Finally, the spectra obtained by FIIST were observed to be consistent with those obtained by the reference Bruker spectrometer.

3.3. Imaging application

The characters *I2M* were printed on a transparency sheet (2 × 2 cm) for laser jet printers, as illustrated in Fig. 7A. FIIST was applied to measure the absorbance as a function of wavelength for the sample. The spectra obtained at three pixels are reported in Fig. 7B, and the analyzed pixel positions are depicted by dots in Fig. 7A. It should be noted that the reported spectra were obtained over a pixel of ink (over the letter M), then over the transparent part (center of the image) and over another pixel far from the light source (corner right). The transparency sheet was composed of polyethylene terephthalate (PET), with characteristic bands at 2460 cm^{-1} (4.06 μm), 2200 cm^{-1} (4.54 μm), 2050 cm^{-1} (4.88 μm) and 1950 cm^{-1} (5.25 μm) [19]. More infrared bands located between 6 to 14μm [20] are required to more precisely characterize the nature of the material in terms of structure and orientation, which can further be correlated to polymer crystallinity. The IR band observed at 2127 cm^{-1} (4.7 μm) may be related to the surface coating over the transparency sheet, which is not specified by the manufacturer. The transparency spectrum shows higher absorbance (Fig. 7B, bold dashed line) than that obtained from the ink pixel (Fig. 7B, dashed line). In addition, the two spectra show the same characteristics bands. In contrast, infrared bands over the wavelength range between 2 and 6.06 μm were observed for the ink. The spectra obtained from the pixel far from the light source, referred to as background (Fig. 7B, solid line), shows that the surrounding signal was insignificant compared with that emitted by the sample. Finally, four images captured at different wavelengths are shown in Fig. 7C to illustrate the FIIST approach. Fig. 7C.1 illustrates the absorbance of the sample at 3.4 μm. At this wavelength, the absorbance is very weak (close to zero), making it difficult to discern the printed characters I2M.

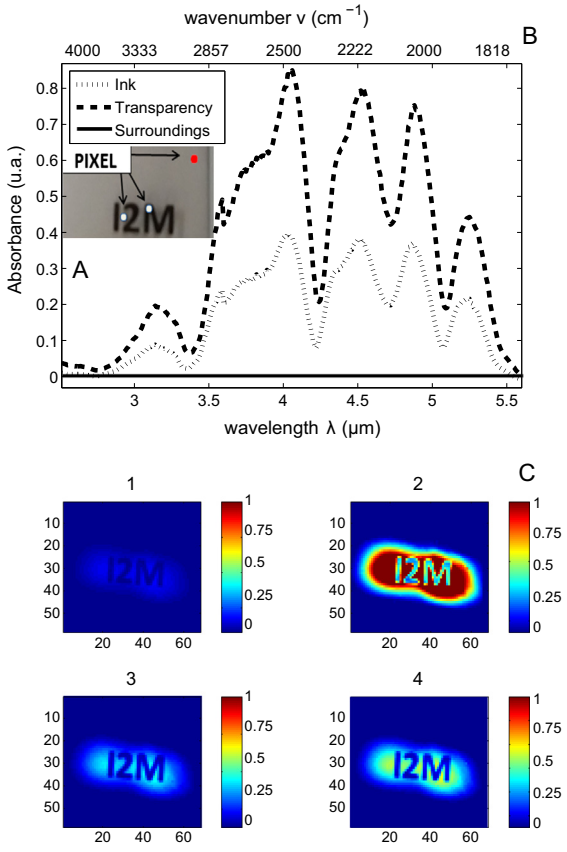

Fig. 7. (A) Visible image of a 2 × 2 cm printed transparency sheet; pixel positions are depicted as dots. (B) Spectra obtained over the transparency sheet (bold dashed line), the ink (dashed line) and another pixel far from the light source, referred to as background (solid line). (C) Infrared images of the sample (original size of the printed transparency sheet) at different wavelengths (1) 3.4 μm, (2) 4.1 μm, (3) 5.1 μm and (4) 5.25 μm.

Fig. 7C.2 illustrates the absorbance of the sample at 4.1 μm. At this wavelength, the absorbance of the transparency is maximal, and high contrast compared with the ink pixel is observed. Fig. 7C.3 and C.4 illustrate, respectively, the absorbance of the sample at 5.1 and 5.25 μm. For visualization purposes, in Fig. 7B, normalized absorbances are reported to enable a direct comparison with the images at each wavelength shown in Fig. 7C. It should be noted that a matrix of 320 × 240 pixels covers a sample surface area of 2 × 2 cm for a spatial resolution of ≈200 μm; furthermore, the spectral analysis was performed in 2.2 min.

4. Conclusions and perspectives

In this paper, the fast infrared spectral imaging technique (FIIST) was presented. The device implementing this technique is based on a Bentham monochromator for sample analysis, combined with an FLIR infrared cooled camera as the sensor. The performance of the instrument was compared with that of a commercial Bruker Vertex 70v spectrometer (used as reference). Thus, it was necessary to choose a high-performance standard reference to enable comparison and thereby best describe the performance of FIIST by applying the reference criteria of the Bruker spectrometer in terms of spectral chemical characterization. Spectroscopy of several materials was performed by both instruments. Based on the results of these experiments, it can be concluded that FIIST enables spectral characterization consistent with that of the reference spectrometer. It was observed that the spectra obtained by FIIST exhibit higher transmittance and provide the possibility of analyzing usually opaque materials in transmission mode. In addition, the FPA technology allows for nearly the same performance as the reference spectrometer (spatial and temporal) to be attained. In contrast, because the Bruker spectrometer was not built for mapping purposes, the mapping of chemicals composition is time-consuming. Therefore, FIIST was designed to generate 76,800 spectra simultaneously to analyze surface areas measuring a few cm^2 in less than 3 min and achieve high rates of spectral acquisition (320 spectra/s).

This work demonstrates that there is no obstacle in performing fast infrared imaging spectroscopy by applying the proposed technique. The results of this study show that this novel technique is a convenient and powerful tool for the characterization of thin films and can be applied to the analysis of heterogeneous materials as well as that of liquids and gases. Future work will involve the extension of the FIIST to MCT camera applications (IR domain 6 to 14 μm) and the development of instrumentation that enables the measurement of concentration (monochromator) and temperature (IR camera) simultaneously. Additionally, a study will be carried out to define the resolution limit of the developed instrument as well as the thickness limit for samples as a function of the optical depth. Note that at longer wavelengths emission from the sample will be an important factor. Furthermore, the most important task that remains is to apply this technique to monitor more complex physical phenomena such as phase changes, kinetics of chemical reactions, and in situ medical applications, phenomena characterized by variations in both temperature and concentration.

Conflict of interest

There is no conflict of interest.

Acknowledgments

The authors gratefully acknowledge L. Lyons and S. Magness from Bentham for their technical and scientific support. This research is based on work supported by the CNRS National Science Foundation under the grant “Instrumentation aux limites” No. 47570.

References

[1] C.D. Tran, Y. Cui, S. Smirnov, Simultaneous multispectral imaging in the visible and near-infrared region: applications in document authentication and determination of chemical inhomogeneity of copolymers, Anal. Chem. 70 (1998) 4701–4708.
[2] M. Kim, A. Lefcourt, K. Chao, Y. Chen, I. Kim, D. Chan, Multispectral detection of fecal contamination on apples based on hyperspectral imagery: Part i. Application of visible and near-infrared reflectance imaging, Trans. Am. Soc. Agric. Eng. 45 (2002) 2027–2038.
[3] V. Ntziachristos, C. Bremer, R. Weissleder, Fluorescence imaging with near-infrared light: new technological advances that enable in vivo molecular imaging, Eur. Radiol. 13 (2003) 195–208.
[4] M. Abedin, I. Bhat, S. Gunapala, S. Bandara, T. Refaat, S. Sandford, U. Singh, The future of single-to multi-band detector technologies, in: Future Trends in Microelectronics: up the Nano Creek, 2007, pp. 335–3476.
[5] C. Ibarra-Castanedo, S. Sfarra, D. Ambrosini, D. Paoletti, B. Bendada, X. Maldague, Subsurface defect characterization in artworks by quantitative pulsed phase thermography and holographic interferometry, Quant. InfraRed Thermogr. J. 5 (2008) 131–149.
[6] F. Cernuschi, P. Bison, A. Figari, S. Marinetti, E. Grinzato, Thermal diffusivity measurements by photothermal and thermographic techniques, Int. J. Thermophys. 25 (2004) 439–457.
[7] M. Niezgoda, D. Rochais, F. Enguehard, P. Echegut, B. Rousseau, Modeling of time-resolved coupled radiative and conductive heat transfer in multilayer semitransparent materials up to very high temperatures, Appl. Phys. Lett. 99 (2011) 224101.
[8] C. Pasquini, Near infrared spectroscopy: fundamentals, practical aspects and analytical applications, J. Braz. Chem. Soc. 14 (2003) 198–219.
[9] G. Reich, Near-infrared spectroscopy and imaging: basic principles and pharmaceutical applications, Adv. Drug Deliv. Rev. 57 (2005) 1109–1143.
[10] A. Rogalski, Infrared Detectors, CRC Press, 2010.

[11] R.C. Lyon, D.S. Lester, E.N. Lewis, E. Lee, X.Y. Lawrence, E.H. Jefferson, A.S. Hussain, Near-infrared spectral imaging for quality assurance of pharmaceutical products: analysis of tablets to assess powder blend homogeneity, AAPS PharmSciTech 3 (2002) 1–15.
[12] D.F. Barbin, G. ElMasry, D.-W. Sun, P. Allen, Non-destructive determination of chemical composition in intact and minced pork using near-infrared hyperspectral imaging, Food Chem. 138 (2013) 1162–1171.
[13] A. Rogalski, K. Chrzanowski, Infrared devices and techniques, Optoelectron. Rev. (2002) 111–136.
[14] M.R. Smith, J.L. Bandfield, E.A. Cloutis, M.S. Rice, Hydrated silica on mars: combined analysis with near-infrared and thermal-infrared spectroscopy, Icarus 223 (2013) 633–648.
[15] J.V. Coe, Z. Chen, R. Li, R. Butke, B. Miller, C.L. Hitchcock, H.C. Allen, S.P. Povoski, E.W. Martin, Imaging infrared spectroscopy for fixation-free liver tumor detection, in: SPIE BiOS, International Society for Optics and Photonics, 2014. pp. 89470B–89470B.
[16] K.A. Chan, S.G. Kazarian, FT-IR spectroscopic imaging of reactions in multiphase flow in microfluidic channels, Anal. Chem. 84 (2012) 4052–4056.
[17] C.-Y. Wei, K. Wang, E. Taft, J. Swab, M. Gibbons, W. Davern, D. Brown, Technology development for InSb infrared imagers, IEEE Trans. Electron Dev. 27 (1980) 170–175.
[18] A. Baldacci, V. Malathy Devi, D.-W. Chen, K. Narahari Rao, B. Fridovich, Absorption spectrum of carbon dioxide at 4.3 μm, J. Mol. Spectrosc. 70 (1978) 143–159.
[19] C.E. Miller, B. Eichinger, Determination of crystallinity and morphology of fibrous and bulk poly (ethylene terephthalate) by near-infrared diffuse reflectance spectroscopy, Appl. Spectrosc. 44 (1990) 496–504.
[20] K.C. Cole, J. Guevremont, A. Ajji, M. Dumoulin, Characterization of surface orientation in poly (ethylene terephthalate) by front-surface reflection infrared spectroscopy, Appl. Spectrosc. 48 (1994) 1513–1521.